A Transformed Isentropic Coordinate and Its Use in an Atmospheric Model

ČEDOMIR BRANKOVIĆ

Hydrometeorological Institute of Croatia, Zagreb, Yugoslavia

(Manuscript received 3 June 1980, in final form 2 April 1981)

ABSTRACT

A primitive equation numerical model utilizing normalized potential temperature as the vertical coordinate is described. This coordinate system enables an easier approach to the treatment of the lower boundary condition in comparison to tne ordinary potential temperature coordinate. For the case of a baroclinically unstable atmosphere, the model has been implemented successfully.

1. Introduction

After the first successful integration of the hydrostatic equations using an isentropic coordinate system (Eliassen and Raustein, 1968), potential temperature is being used increasingly as a vertical coordinate in analyzing and forecasting atmospheric processes. Thus, Rossby's (1937) arguments for the isentropic system have won a high reputation in numerical modeling especially for research purposes. Moreover, in many cases, for example, in the investigations of frontal zones, this coordinate system has several advantages over other widely used systems utilizing either geometrical height or pressure as a vertical coordinate.

A number of papers treating potential temperature as a vertical coordinate in numerical models have been published in the last decade (e.g., Bleck, 1973, 1974, 1977; Eliassen and Raustein, 1970; Shapiro, 1975, 1976; Trevisan, 1976, and others). Bleck and Shapiro (1976) gave a systematic review of advantages and disadvantages of the isentropic coordinate models.

To overcome the disadvantage of isentropes intersecting the surface of the earth, Kasahara (1974) proposed the use of normalized potential temperature as vertical coordinate in a numerical model. In this case the earth's surface becomes a coordinate surface.

Since the vertical coordinate defined above follows directly from the potential temperature, it retains many of the advantages of potential temperature as vertical coordinate. The main advantages of the θ vertical coordinate are a higher vertical resolution and weaker horizontal gradients of velocity in frontal zones in comparison to p or z coordinates. It seems these advantages are partly lost in going to the normalized θ coordinate. However, as long as surface potential temperature gradients are holding relatively smooth, the angle between θ surfaces and normalized θ surfaces is small and a loss of the features mentioned above is not significant. This is illustrated in Fig. 1 which shows the same vertical cross section presented as Fig. 2 in the paper by Bleck and Shapiro (1976).

The purpose of this work is to describe the new vertical coordinate and a numerical model using this vertical coordinate. In the following section theoretical considerations and finite-difference methods are given. After that the testing of the model and results are described.

2. Theoretical and numerical approach

a. Definition of normalized potential temperature and basic equations

A normalized isentropic coordinate can be defined by the expression

$$\eta = \frac{\theta - \theta_T}{\theta_S - \theta_T}, \tag{2.1}$$

where θ is potential temperature, θ_T a constant potential temperature at the top of the atmospheric model and θ_S a variable potential temperature at the earth's surface. Assuming that θ increases monotonically with height then $\theta_T > \theta_S$ and $\eta = 0$ at $\theta = \theta_T$ and $\eta = 1$ at $\theta = \theta_S$; thus, the η coordinate decreases continuously from the earth's surface to the top of the model. In the definition (2.1) both the denominator and numerator are negative. Taking the former assumption the η coordinate is always positive. A similar definition was derived by Kasahara, the only difference being that the numerator and denominator are the differences between θ_T and θ, and θ_T and θ_S, respectively, i.e., these differences are positive. However, the definition

0027-0644/81/092029-11$06.75

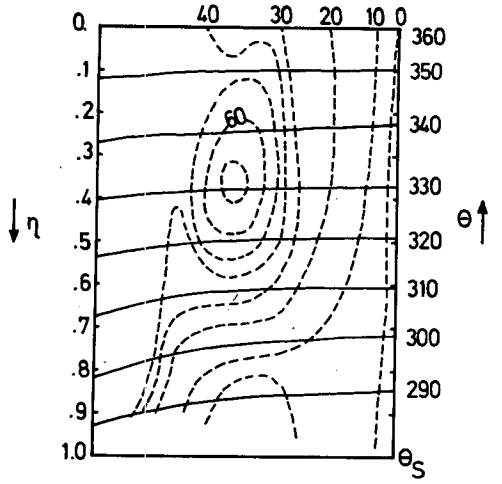

FIG. 1. Frontal zone and θ surfaces in normalized potential temperature coordinate.

(2.1) is similar to the definition of the σ coordinate, well-known normalized coordinate in the p system.

The momentum equation has the form

$$\frac{d\mathbf{V}}{dt} = -f\mathbf{k} \times \mathbf{V} + \Pi\eta\nabla\theta_S - \nabla_\eta M + \mathbf{F}, \quad (2.2)$$

where $\mathbf{V}$ denotes horizontal velocity, f the Coriolis parameter, Π the Exner function ($\Pi = c_p[p/p_0]^\kappa$, where c_p is the specific heat at constant pressure, p pressure, $p_0 = 1000$ mb, $\kappa = R/c_p = 0.286$ and R the gas constant), M is the Montgomery potential ($M = c_pT + gz$, where T is temperature, g earth's gravity and z geometrical height), and $\mathbf{F}$ denotes the frictional force per unit mass. The total derivative is given by

$$\frac{d}{dt} = \left(\frac{\partial}{\partial t}\right)_\eta + \mathbf{V}\cdot\nabla_\eta + \dot{\eta}\frac{\partial}{\partial\eta}, \quad (2.3)$$

where $\dot{\eta} = d\eta/dt$ denotes vertical velocity. Using the definition (2.1), we obtain

$$\dot{\eta} = \frac{1}{\theta_S - \theta_T}\left(\frac{d\theta}{dt} - \eta\frac{d\theta_S}{dt}\right). \quad (2.4)$$

Here $d\theta/dt$ and $d\theta_S/dt$ are individual changes of potential temperature at any η level and at the earth's surface, respectively, which can be expressed by the first law of thermodynamics.

The hydrostatic equation is given by

$$\frac{\partial M}{\partial\eta} = \Pi(\theta_S - \theta_T). \quad (2.5)$$

By integrating (2.5) with respect to η from the earth's surface to any η level we obtain a diagnostic equation for M in the form

$$M = M_S + (\theta_S - \theta_T)\int_1^\eta \Pi d\eta, \quad (2.6)$$

where M_S denotes the Montgomery potential at the earth's surface

$$M_S = \Pi_S\theta_S + gH, \quad (2.7)$$

where Π_S is the Exner function at the earth's surface and H is topography.

The continuity equation in the η coordinate system has the form

$$\frac{\partial}{\partial\eta}\left(\frac{\partial p}{\partial t}\right)_\eta + \nabla_\eta\cdot\left(\mathbf{V}\frac{\partial p}{\partial\eta}\right) + \frac{\partial}{\partial\eta}\left(\dot{\eta}\frac{\partial p}{\partial\eta}\right) = 0. \quad (2.8)$$

By integrating (2.8) with respect to η from the bottom to the top of the atmospheric model and taking into consideration the upper and the lower boundary conditions

$$\dot{\eta} = 0 \quad \text{at} \quad \eta = \eta_T = 0,$$
$$\dot{\eta} = 0 \quad \text{at} \quad \eta = \eta_S = 1,$$

we obtain the surface pressure tendency equation

$$\frac{\partial p_S}{\partial t} = \frac{\partial p_T}{\partial t} - \int_0^1 \nabla_\eta\cdot\left(\mathbf{V}\frac{\partial p}{\partial\eta}\right)d\eta, \quad (2.9)$$

where p_T denotes pressure at the model's top and p_S is the surface pressure.

The thermodynamic equation can be derived from the convenient form $c_p d(\ln\theta)/dt = dS/dt$, where S denotes entropy. The right-hand side can be expressed as $dS/dt = \dot{Q}/T$, where $\dot{Q}$ stands for the rate of heating (cooling) per unit mass per unit time. Thus, we have

$$\frac{d\theta}{dt} = \frac{\dot{Q}}{\Pi}. \quad (2.10)$$

Vertical velocity (2.4) is completely defined when (2.10) is known.

As pointed out by Kasahara, we need an additional upper boundary condition to keep the vertically integrated total energy equation in conservation law form. We can choose either the height z_T of the model's top as a constant for $\eta = \eta_T$ or $\partial p_T/\partial t = 0$ at $\eta = \eta_T$. If we should decide

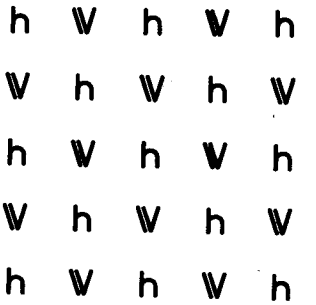

FIG. 2. Spatial distribution of dependent variables over the (E) grid.

for the first case then we have to calculate $\partial p_T/\partial t$, i.e., pressure tendency at the top of the model. It includes additional considerations and derivations and thus we shall solve for the latter, more convenient, case.

b. The model

To generate a simple model in η coordinates it is convenient to make some assumptions. The first one is that the motions are adiabatic. Most of equations reduce to a simple form. Furthermore, we neglect the frictional force and rewrite the prognostic equations in the η system as following:

1) THE MOMENTUM EQUATION

$$\frac{d\mathbf{V}}{dt} = -f\mathbf{k} \times \mathbf{V} + \Pi\eta\nabla\theta_S - \nabla_\eta M. \quad (2.11)$$

2) THE EQUATION OF CONTINUITY

$$\frac{\partial}{\partial\eta}\left(\frac{\partial p}{\partial t}\right)_\eta + \nabla_\eta \cdot \left(\mathbf{V}\frac{\partial p}{\partial \eta}\right) = 0. \quad (2.12)$$

The above equation is integrated with respect to η to give

$$\frac{\partial p}{\partial t} = -\int_0^\eta \nabla_\eta \cdot \left(\mathbf{V}\frac{\partial p}{\partial \eta}\right). \quad (2.13)$$

3) THE EQUATION OF THERMODYNAMICS

$$\frac{d\theta}{dt} = 0. \quad (2.14)$$

c. Finite-difference formulation

The model atmosphere is divided by several η levels which are carrying velocity components and pressure as historic variables. At the model's top θ_T and p_T are kept constant. Because the potential temperature θ at every grid point at every η level is known from (2.1) and therefore θ_S values are required, the equation of thermodynamics simply reduces to the equation for the advection of the surface potential temperature

$$\frac{\partial\theta_S}{\partial t} = -u_S\frac{\partial\theta_S}{\partial x} - v_S\frac{\partial\theta_S}{\partial y}, \quad (2.15)$$

where u_S and v_S are zonal and meridional surface wind components, respectively.

By integrating (2.12) with respect to η between any two levels and summing from the top to the bottom of the model we obtain the vertically differentiated equation of the surface pressure tendency

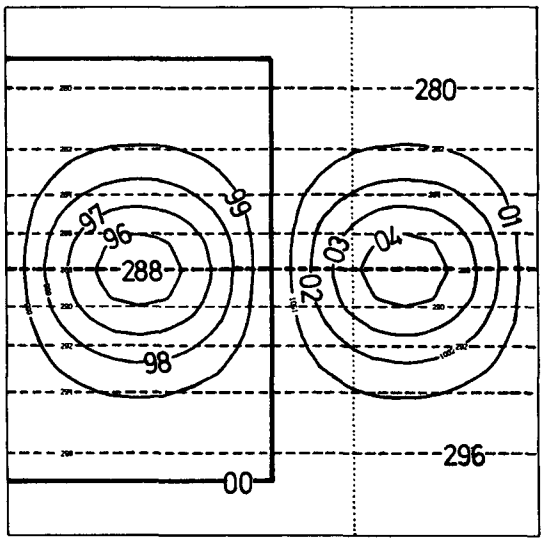

FIG. 3. Initial surface pressure (solid) and surface potential temperature (dashed). Heavy solid line denotes 1000 mb and its shape is due to plotter decision. Dotted line indicates position of vertical cross section.

$$\frac{\partial p_S}{\partial t} = -\frac{1}{2}\sum_{k=1}^{k=LM-1}\left\{(u_k + u_{k+1})\frac{\partial}{\partial x}(p_{k+1} - p_k) + (v_k + v_{k+1})\frac{\partial}{\partial y}(p_{k+1} - p_k) + (p_{k+1} - p_k) \times \left[\frac{\partial}{\partial x}(u_k + u_{k+1}) + \frac{\partial}{\partial y}(v_k + v_{k+1})\right]\right\}, \quad (2.16)$$

where LM denotes the maximum number of η levels and k and $k + 1$ are the upper and lower computational levels.

The horizontal grid [the (E) grid in Fig. 2] follows the notation used by Mesinger and Arakawa (1976) and the horizontal scheme is a centered finite-difference scheme. The main reason for this lattice is its good characteristics for simulation of the geostrophic adjustment process.

For time differencing the leapfrog scheme was adopted except in the first time step when a forward step was used. To overcome the difficulty with decoupling of the gravity wave solutions on the elementary subgrids, Janjić's (1974) technique was applied.

A typical time integration step is as follows. First, diagnostic variables, the Exner function and the Montgomery potential are computed. Then prognostic arrays, wind components from the momentum equation, pressure from the equation of continuity and, finally, surface potential temperature from the equation of thermodynamics are calculated.

3. Experiments and results

The model is developed in a β channel centered at 45°N. The channel dimensions are 4000 × 4000 km. In the preliminary experiments the nearest distance between two h points on the (E) grid was $100\sqrt{2} \approx 141.421$ km and time step was 2.5 min. Free-slip conditions along the northern and the southern walls and cyclic boundary conditions in the west–east direction are applied. The vertical structure is determined by five η levels defined at 0.1, 0.3, 0.5, 0.7 and 0.9.

The model has been tested using the baroclinically unstable atmosphere described by Eliassen and Raustein (1970, hereafter referenced as ER), the only difference being that the average surface potential temperature is 288 K.

Preliminary integrations showed that on the northern and southern boundaries an instability was generated. It expanded relatively rapidly to the inner points and the surface pressure tendencies computed at every time step were large. The model failed after 18 h of simulated time.

Testing of the model finite-difference equations was thus performed by an experiment with the barotropic atmosphere. It was found that the Laplacian terms in the finite-difference form of the pressure tendency equation, i.e.,

$$p_l^{\tau+1} = p_l^{\tau-1} - \Delta t \sum_{k=1} \{(\bar{u}_k^{xy} + \bar{u}_{k+1}^{xy})\overline{\delta_x(p_{k+1} - p_k)}^{xy} + (\bar{v}_k^{xy} + \bar{v}_{k+1}^{xy})\overline{\delta_y(p_{k+1} - p_k)}^{xy} + (p_{k+1}^{\tau} - p_k^{\tau})[(\delta_x u_x^{\tau} + \delta_y v_k^{\tau}) + (\delta_x u_{k+1}^{\tau} + \delta_y v_{k+1}^{\tau}) + w\Delta t(\eta_k \Pi_k^{\tau-1} + \eta_{k+1}\Pi_{k+1}^{\tau-1})(\nabla_\times^2 - \nabla_+^2)\theta_S^{\tau-1} - w\Delta t(\nabla_\times^2 - \nabla_+^2)(M_k^{\tau-1} + M_{k+1}^{\tau-1})]\}, \quad (3.1)$$

caused enormous values of the surface pressure tendencies at the boundaries. In the above expression τ denotes time level, w is a parameter, Δt the time step, and $\nabla_\times^2$ and ∇_+^2 are the two alternative finite-difference Laplacian operators introduced by Janjić to avoid decoupling of gravity waves. The bar denotes the averaging procedure on the (E) grid.

To overcome this problem linear extrapolation for M and θ_S at the fictitious h points outside the lateral boundaries was introduced. In this case the model from the initially barotropic stage integrated over 48 h of simulated time, and the experimentation with the initially baroclinic atmosphere was recommended.

The initial wind field for the baroclinic experiment was computed according to the geostrophic wind relation

$$\mathbf{V}_g = f^{-1}\mathbf{k} \times \nabla_\eta \mathbf{M} - \Pi\eta f^{-1}\mathbf{k} \times \nabla\theta_S. \quad (3.2)$$

As happened in the barotropic case, over 48 h of integration was completed before computational instability occurred. A further substantial stabilization of the integration scheme was then obtained by removing the Laplacian terms in (3.1) from the first two boundary row points at the northern and at the southern boundary.

The original channel width was 3000 km (the first trial, later called the "narrow" channel). In this case, as happened in ER, as simulated time came closer to the end of integration (over four days) the cold air concentrated along the southern boundary. Thus, there was no possibility for the free development of the cold front in the vicinity of the southern boundary. To avoid this problem, the channel width was extended to 4000 km. However, the meridional gradients of the surface potential temperature and the surface pressure in the regions 1500 km northward and 1500 km southward from the channel central line were kept as in the "narrow" channel. In the extended regions 500 km northward and 500 km southward the surface potential temperature and the surface pressure were constant with the same values as at the lateral boundaries in the "narrow" channel version (Fig. 3). The meridional vertical cross section (Fig. 4) shows the initial vertical structure of the model atmosphere along the line 2600 km westward from the channel starting point

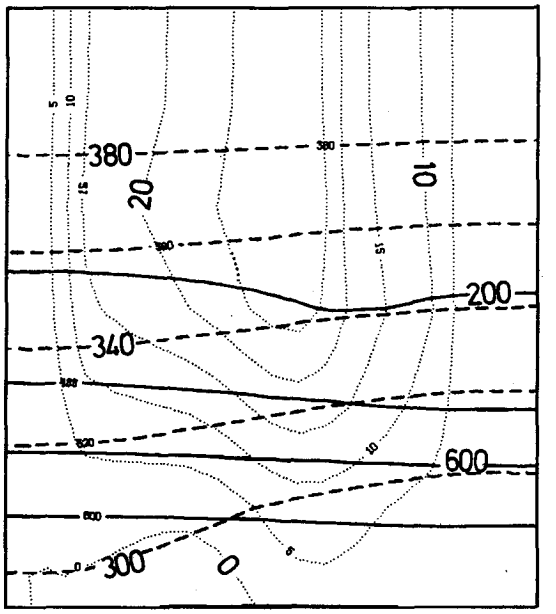

FIG. 4. Initial meridional vertical cross section. Solid lines are isobars, dashed lines isentropes and dotted lines zonal wind. North is on the right-hand side.

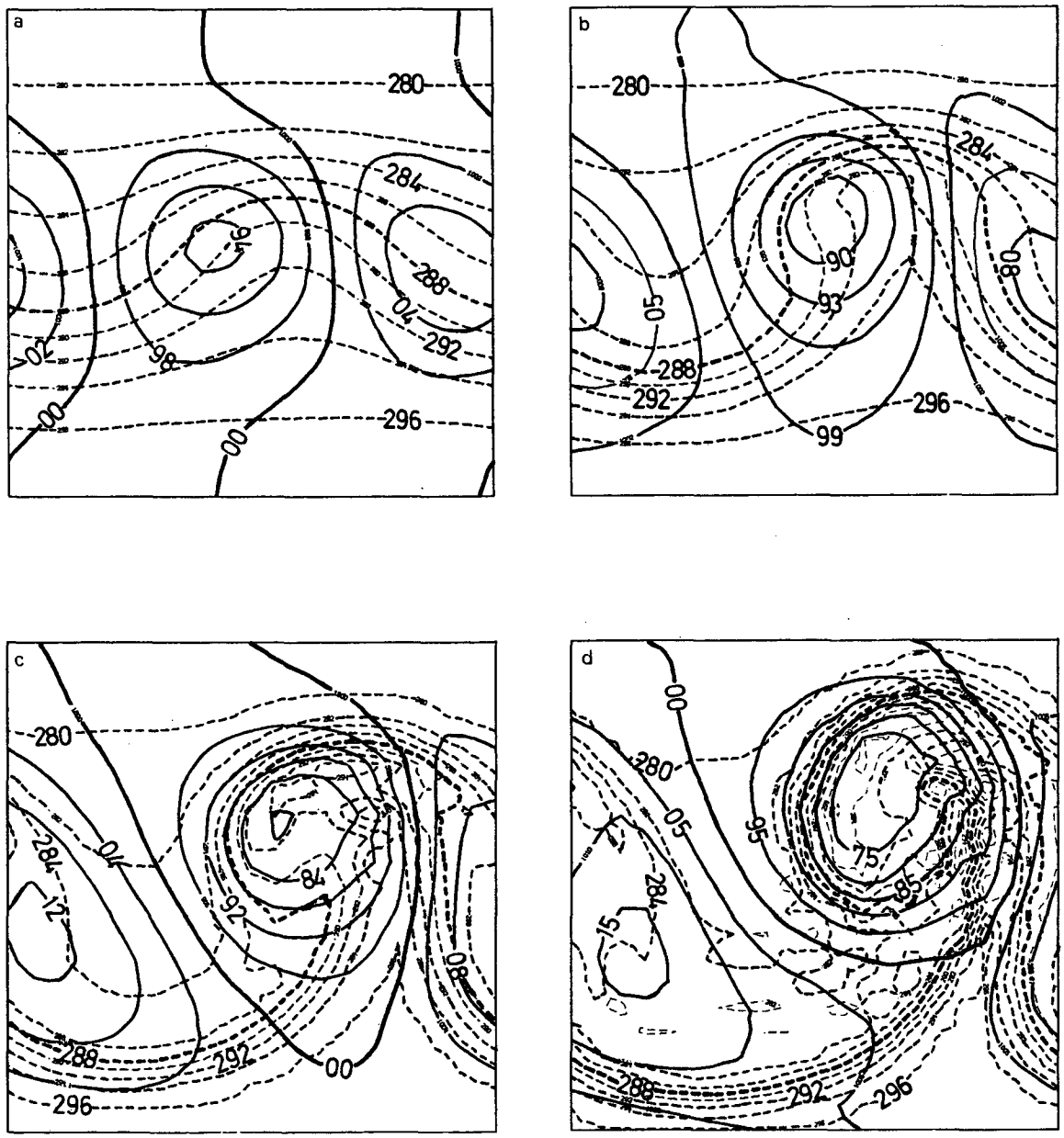

FIG. 5. Surface forecast presented at 24 h intervals. Isopleths as in Fig. 3.

as indicated in Fig. 3. The slope of isentropes is the consequence of the surface temperature distribution. The sagging of the 200 mb level indicates the presence of the tropopause in whose vicinity strong wind occurs.

The results of the model time integration are shown in Fig. 5. A considerable, meteorologically significant and quite realistic development from the initial low–high system is noticeable. After 24 h a thermal ridge has been formed due to initial circulation (Fig. 5a). In Fig. 5b the thermal ridge becomes a tongue of warm air. The low moves eastward and deepens. At this stage the warm front in the northern part and cold front in the southwestern part are in the establishing conditions. After three days there is strong cold front near the southern boundary. The tongue of warm air becomes narrower and we can say that the model simulates an occlusion process. Fig. 5d shows thermal and pressure fields a few hours before the termination of the time integration. The isobars and the isotherms coincide over most of the β channel and one cannot expect any further development. After four days the low has decreased from 995.4 mb initially to 970.4 mb, and the high has increased from 1004.6 to 1015.9 mb.

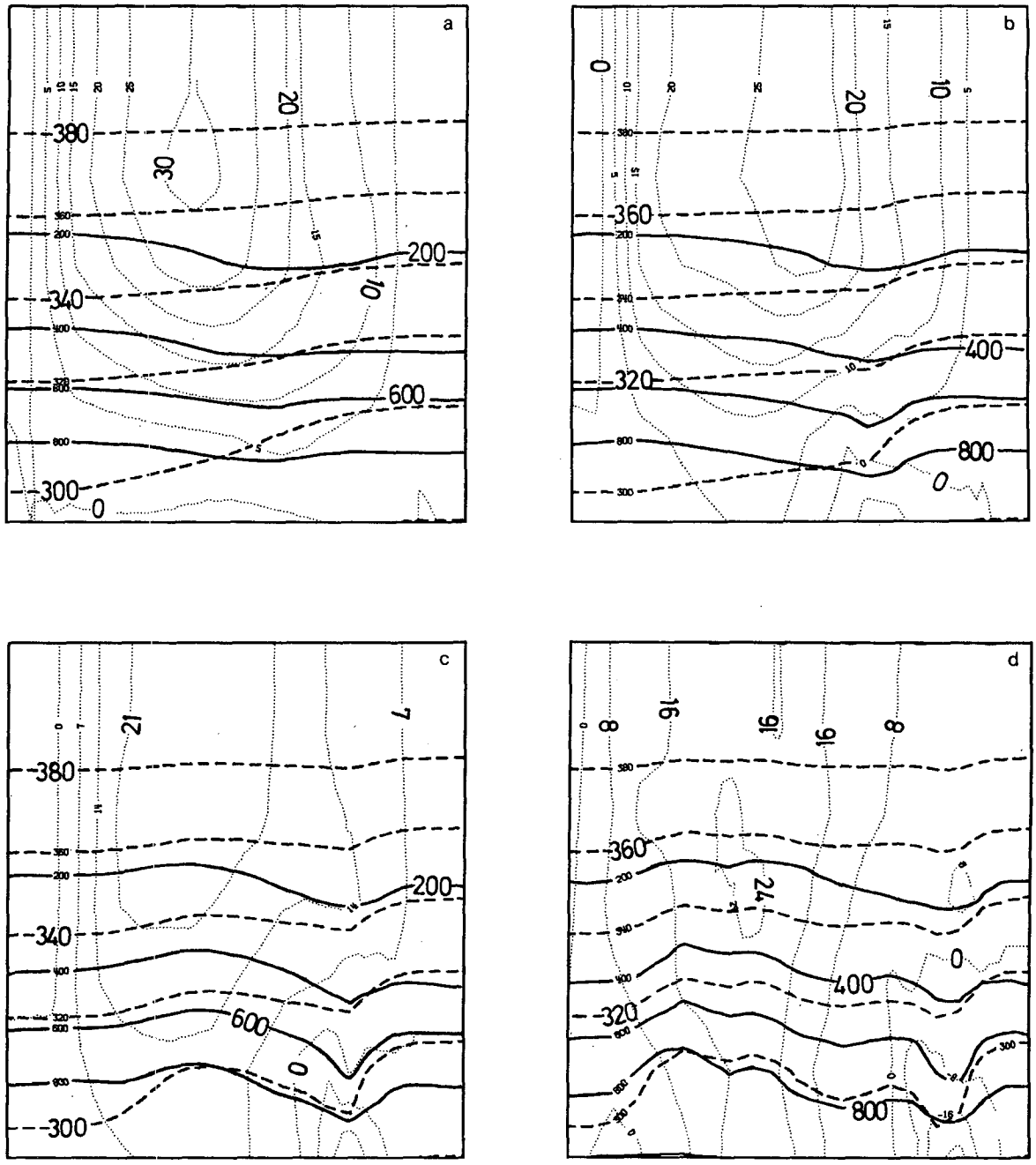

FIG. 6. Vertical cross section at 24 h intervals. Isopleths as in Fig. 4.

Some detailed insight into the atmospheric structure is given in Fig. 6. After 24 h (Fig. 6a) the slope of the 300 K isentrope slightly changes northward due to the strong warm advection in the lower troposphere. The sagging of the isobars throughout the entire cross section is the consequence of the low approaching the line at 2600 km. In the upper atmosphere a jet stream is generated. Fig. 6b shows that the slope of isentropes in the northern region becomes gradually larger and indicates the warm front formation. After 72 h (Fig. 6c) the low and the associated frontal systems are in the stage of full development. The warm front is represented by very strong inclination of isentropic levels, while at the same time in the southern region a somewhat weaker inclination occurs and denotes the cold front. In the northern part of the cyclone easterly zonal wind is noticeable. Finally, after 96 h (Fig. 6d) a perturbation due to numerical instability has an effect on the slope of isolines and contaminates further develop-

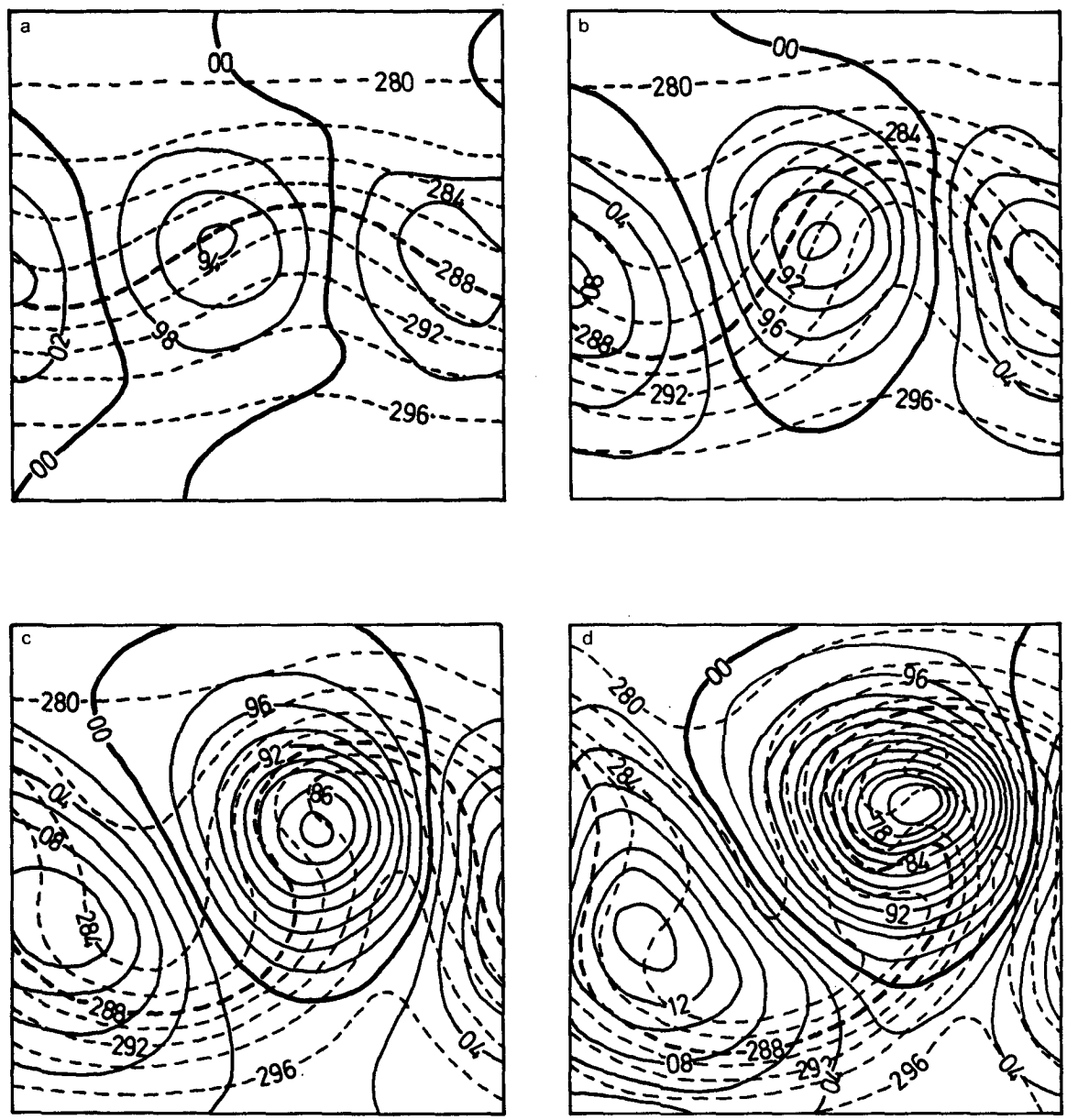

FIG. 7. Surface forecast in the model with $K = 10^6$ m^2 s^{-1} at 24 h intervals. Isopleths as in Fig. 3.

ment. A strong surface potential temperature gradient caused η surfaces to steepen and it was the reason that the model failed.

A further experimentation with the aim to remove instability has continued. Obviously, since the model has not had any smoothing and the instability arose in the thermal field, some kind of diffusion in the equation of thermodynamics should be introduced. Thus, the diffusion term of the form $K\nabla^2\theta_S$ was calculated at every time step with $K = 10^6$ m^2 s^{-1}.

It is necessary to emphasize that experiments including diffusion, due to computer restrictions, were carried out both with doubled grid and time steps.

An essential improvement on the third and the fourth day of the forecasting period can be noticed from Fig. 7. Thus, the low-high system has not developed to the same extent as it did in Fig. 5. Pressure at the low center after 96 h is over 5 mb higher than in the experiment without diffusion. Of greater significance is the fact that the surface potential temperature gradient is not as marked, although a clear difference between the cold air mass at the rear of the low and warm advection is noticeable. In spite of smoothing the frontal zones retain their features. A number of closed isotherms in the surface potential temperature field, the re-

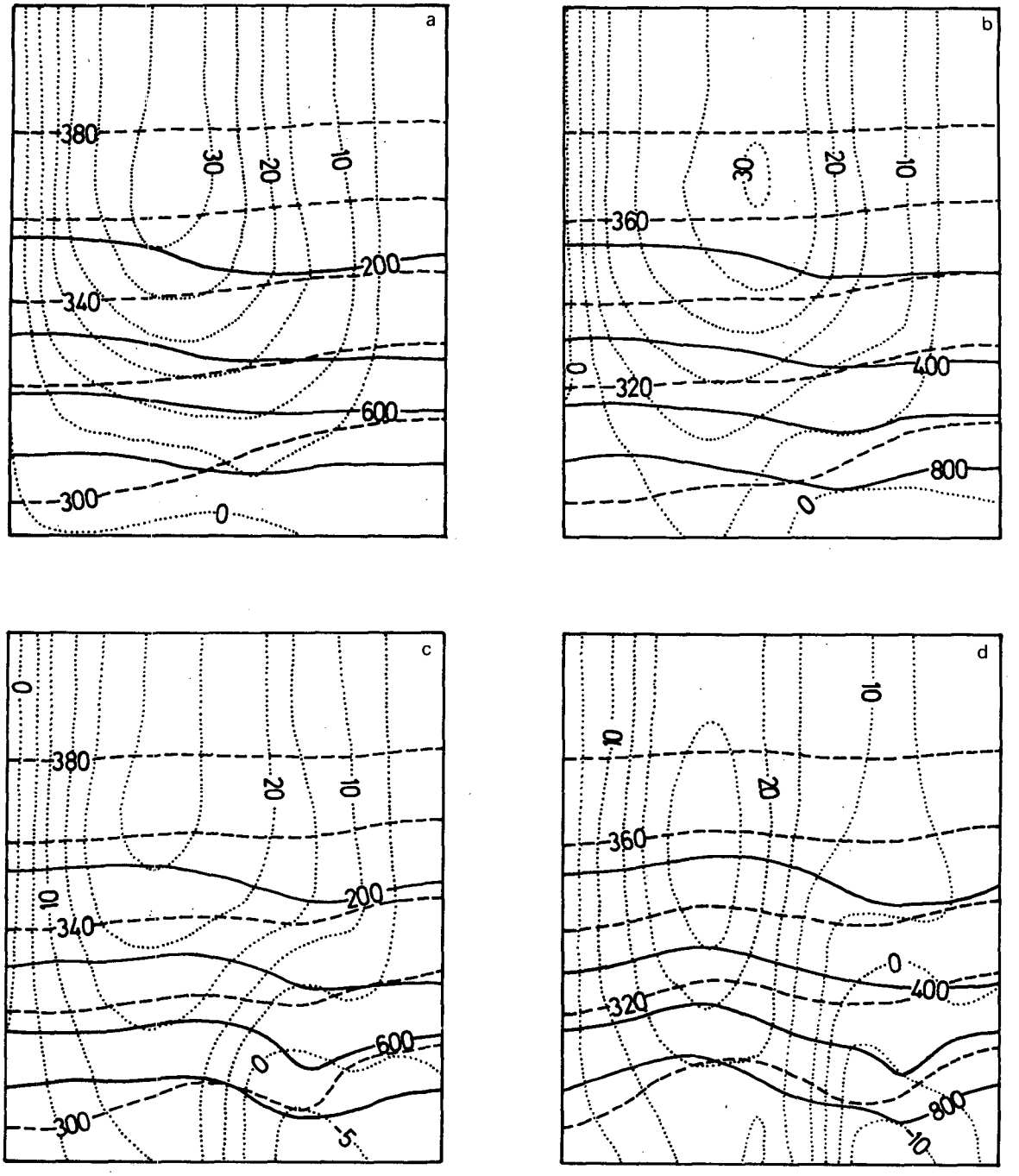

FIG. 8. Vertical cross section in the model with $K = 10^6$ m^2 s^{-1} at 24 h intervals. Isopleths as in Fig. 4.

liable indicators of instability, do not appear in Fig. 7d.

In comparison to Fig. 6, a vertical cross section on the fourth day (Fig. 8d) indicates, more briefly, that there is no instability. The general features of the fields shown resemble that in the experiment without diffusion (and one should not expect any drastic change), but the improvements are obvious. However, as mentioned above, there was no possibility of testing the duration of simulated time longer than four days to prove that instability has been eliminated completely.

Since it was shown that the use of diffusion is physically and numerically suitable, the next experiments were carried out to find to what extent diffusion has an influence on the forecast and to find what amounts of K are allowed.

Two further experiments were carried out. In the

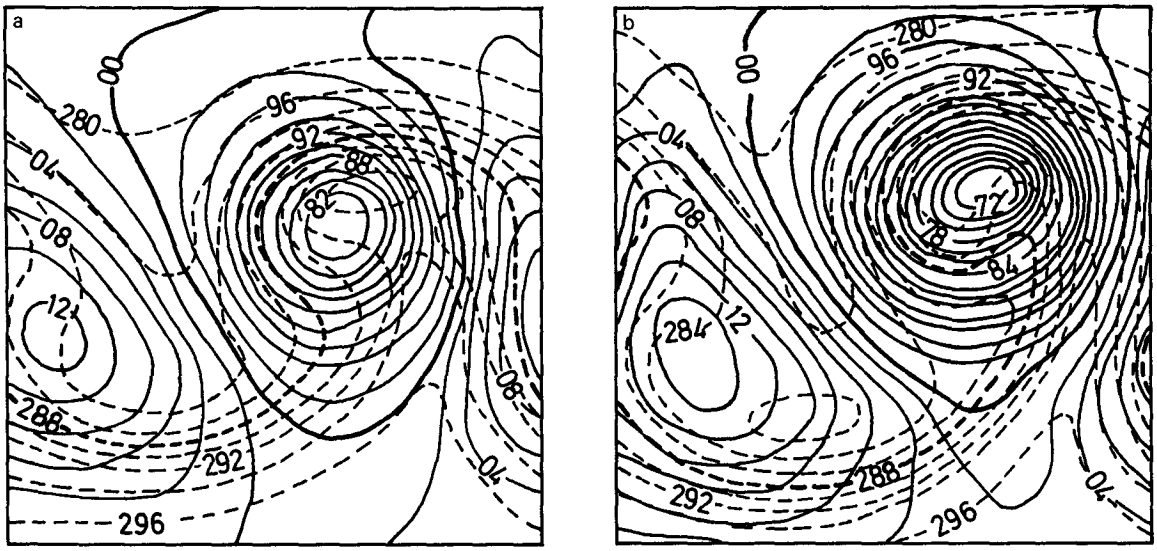

FIG. 9. 72 and 96 h surface forecasts in the model with $K = 10^6$ m^2 s^{-1} included after 48 h of simulation. Isopleths as in Fig. 3.

first one, diffusion with the same coefficient $K = 10^6$ m^2 s^{-1} was introduced after 48 h of simulated time and was calculated at every time step up to the end of integration. The results of 72 and 96 h surface forecasts are presented in Fig. 9. The development of the eastward moving cyclone is somewhat more intense in comparison to Figs. 7c and 7d. After 96 h there is no $\theta_S = 294$ K warm core in the vicinity of the low center, and this feature seems to be more acceptable than in Fig. 7d. However, another unfavorable trait, stronger surface frontal gradients, have already appeared by the third day.

Surface potential temperature gradients in the next experiment which includes diffusion with $K = 10^8$ m^2 s^{-1} but only once (at the end of the second day) are even worse (Fig. 10). This figure is similar to Figs. 5c and 5d. Furthermore, the surface pressure amplitude increased over 50 mb within four days (approximately 45 mb in Fig. 5 and 40 mb in Fig. 7).

Thus the additional experiments show in a rather less sophisticated way the relatively high model sensitivity to the variation of K. Moreover, the determination of the most acceptable value of K was tedious since a number of the model runs had to be made.

Fig. 11 makes it possible to determine the effect of diffusion at every time step from the beginning of the time integration. The energy diagram shows

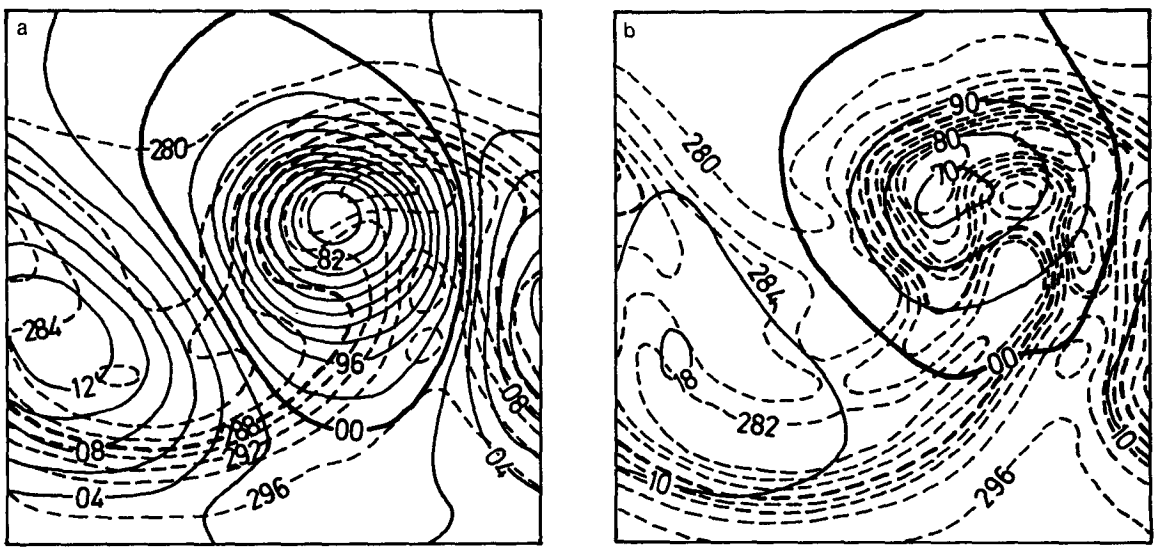

FIG. 10. As in Fig. 9 except for $K = 10^8$ m^2 s^{-1}.

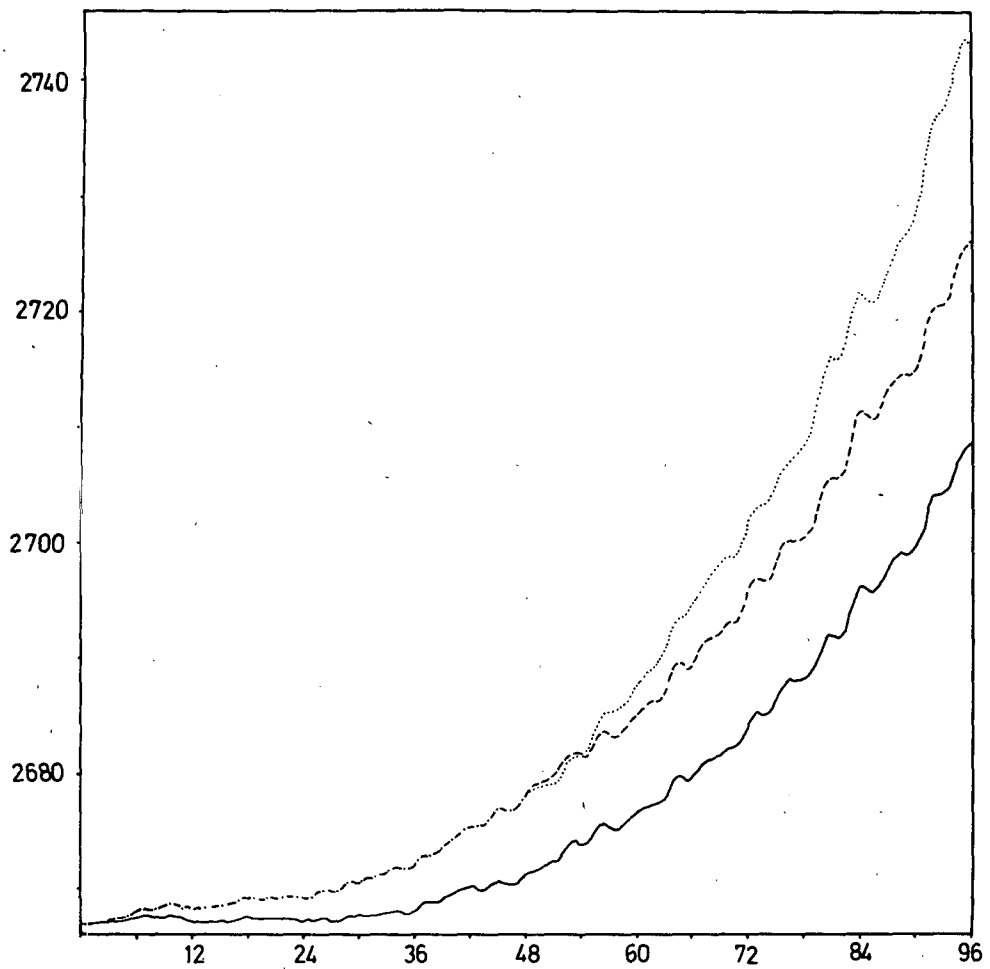

FIG. 11. Average available potential energy plus average kinetic energy per unit mass in simulated time. Solid line indicates the experiment including diffusion at every time step, dashed line at every time step but after 48 h, and dotted line is for the experiment with $K = 10^8$ m^2 s^{-1}.

that an increase of the average available potential energy plus the average kinetic energy at the end of the fourth day in this experiment is near 1.5% of the initial value.

In comparison to ER, we should refer to the experiment presented in Fig. 7. Surface pressure amplitude, i.e., the difference in surface pressure between high and low centers is 2 mb smaller for the normalized θ coordinate. Thus, one might argue that the development is somewhat less pronounced. It should be pointed out, however, that the η model includes smoothing only in the equation of thermodynamics.

The ER amplification was most rapid from 24 to 48 h while in the model presented it was from 72 to 96 h. The variety in the low-high system development becomes obvious when the stages after 48 h are compared. This stage in ER resembles that after 72 h in the present paper.

One of the essential similarities is that in the occlusion process the warm air does not leave the earth's surface. Moreover, the region of $\theta_S > 290$ K seems to be somewhat wider than in ER.

4. Conclusion

A primitive equation numerical model utilizing normalized potential temperature as the vertical coordinate has been proposed, described and tested. There was no problem of isentropes intersecting the surface of the earth, so the treatment of the lower boundary condition appeared to be very easy. No additional mathematical requirements and numerical computations are needed. The equation of thermodynamics is explicitly solved only at the surface of the earth.

This sort of model construction permits a realistic development of the initially baroclinic low–high system. The vertical cross sections show the great advantage of the proposed coordinate, especially in frontal analysis. The shape of isentropes indicates the frontal location while the slope of the

isentropes indicates the frontal intensity. The model energy stability has been demonstrated.

At the present stage the model effectiveness seems to be conditionally satisfying. However, the basic purpose of showing further possibilities of an isentropic coordinate was handled quite satisfactorily.

A very important problem, which has not been treated explicitly, should be pointed out. It is a problem of calculation of the pressure gradient force in the η system and, in principle, the same problem as in any σ model. The pressure gradient force is the sum of two terms with the compensation effect

$$\Pi\eta\nabla\theta_S - \nabla_\eta M. \tag{4.1}$$

In the presence of strong surface potential temperature gradients a relatively small error in one of these terms may produce a large error in the sum. Moreover, similar effects could be expected when topography is included.

Although in the present paper this problem was avoided to some extent by smoothing in a thermal field, it is not definitely solved. However, in the preliminary experiment in which a barotropic atmosphere with a uniform zonal flow was considered, the cancellation of the two terms in (4.1) for the meridional component of the pressure gradient force was proved. This result should not be generalized and a further examination is warranted.

The comparison (or calculation) of the two relatively "less convenient variables", θ_S and M, in (4.1) might be overcome by taking into consideration that at any η level $M = \Pi\theta + \phi$, where ϕ stands for geopotential. Thus, from (4.1) it follows that a new expression for the pressure gradient force

$$-\theta\nabla_\eta\Pi - \nabla_\eta\phi,$$

in which the Exner function (i.e., pressure) and geopotential are physically more convenient values, could be examined. Furthermore, the question of how to determine geopotential at η levels could be answered if an alternative form of the hydrostatic equation in the θ system, according to Eliassen and Raustein (1968),

$$\frac{\partial\phi}{\partial\Pi} = -\theta \tag{4.2}$$

is considered. Transformation of (4.2) to η coordinates yields

$$\frac{\partial\phi}{\partial\eta} = -\theta\frac{\partial\Pi}{\partial\eta}. \tag{4.3}$$

By integrating (4.3) with respect to η from the bottom to any η level the value of ϕ can be obtained.

Other possible methods, like in σ coordinates, for solving existing problems should be suggested. In any case great care is needed if one demands an accurate computation of the pressure gradient force in the regions of strong thermal gradients.

Thus, the next test of this or any other numerical model using η coordinates ought to be the simulation of the atmosphere in the presence of topography with special reference to the problem of the pressure gradient force. The inclusion of topography seems to be relatively straightforward. The results presented here give a possibility of a new application of potential temperature coordinate in numerical modeling.

Acknowledgments. The experimental part of this work was partially completed during the author's May–July 1979 visit to the European Centre for Medium Range Weather Forecasts, a facility organized and supported by the British Council. The author expresses gratitude to his ECMWF supervisor Dr. A. Simmons. He also wishes to thank Drs. D. Burridge and S. Tibaldi for their helpful discussions and suggestions.

The continuation of the work was supported by the Republican Association for Scientific Research of Croatia.

REFERENCES

Bleck, R., 1973: Numerical forecasting experiments based on the conservation of potential vorticity on isentropic surfaces. *J. Appl. Meteor.*, **12**, 737–752.

——, 1974: Short-range prediction in isentropic coordinates with filtered and unfiltered models. *Mon. Wea. Rev.*, **102**, 813–829.

——, 1977: Numerical simulation of lee cyclogenesis in the Gulf of Genoa. *Mon. Wea. Rev.*, **105**, 428–445.

——, and M. A. Shapiro, 1976: Simulation and numerical weather prediction framed in isentropic coordinates. *Weather Forecasting and Weather Forecasts: Models, Systems and Users*, Vol. 1., NCAR Summary Colloqium, 154–169.

Eliassen, A., and E. Raustein, 1968: A numerical integration experiment with a model atmosphere based on isentropic coordinates. *Meteor. Ann.*, **5**, 45–63.

——, and ——, 1970: A numerical integration experiment with a six-level atmospheric model with isentropic information surface. *Meteor. Ann.*, **5**, 429–449.

Janjić, Z. I., 1974: A stable centered difference scheme free of two-grid-interval noise. *Mon. Wea. Rev.*, **102**, 319–323.

Kasahara, A., 1974: Various vertical coordinate systems used for numerical weather prediction. *Mon. Wea. Rev.*, **102**, 509–522.

Mesinger, F., and A. Arakawa, 1976: Numerical methods used in atmospheric models, Vol. 1. *GARP Publ. Ser.*, No. 17, 64 pp.

Rossby, C.-G., and collaborators, 1937: Isentropic analysis. *Bull. Amer. Meteor. Soc.*, **18**, 201–209.

Shapiro, M. A., 1975: Simulation of upper-level frontogenesis with a 20-level isentropic coordinate primitive equation model. *Mon. Wea. Rev.*, **103**, 591–604.

——, 1976: The role of turbulent heat flux in the generation of potential vorticity in the vicinity of upper-level jet stream systems. *Mon. Wea. Rev.*, **104**, 892–906.

Trevisan, A., 1976: Numerical experiments on the influence of orography on cyclone formation with an isentropic primitive equation model. *J. Atmos. Sci.*, **33**, 768–780.